Final Technique Report

Grant Award Numbers:	G12AP20090
Title:	Testing Static vs. Dynamic Triggering Based on Systematic Detection of Missing Triggered Events in Central California
Investigators:	Zhigang Peng Georgia Institute of Technology 311 Ferst Drive Atlanta, GA, 30332-0340 Phone: (404) 894-0231, Fax: (404) 894-5638 zpeng@gatech.edu
Term Covered by the Report:	June 1, 2012 - July 31, 2013
Funding expended	$62,903

Testing Static vs. Dynamic Triggering Based on Systematic Detection of Missing Triggered Events in Central California

Investigations undertaken

Earthquakes trigger other earthquakes, but the physical mechanism of the triggering is currently debated. Most studies of earthquake triggering rely on earthquakes listed in catalogs, which are known to be incomplete around the origin times of large earthquakes, and therefore missing potentially triggered events. Here we apply a waveform matched filter technique to systematically detect earthquakes along the Parkfield section of the San Andreas Fault from 46 days before to 31 days after the nearby 2003 M_w6.5 San Simeon earthquake. After removing all possible false detections, we identify ~8 times more earthquakes than in the Northern California Seismic Network catalog. The newly identified events along the creeping section of the San Andreas Fault show a statistically significant decrease following the San Simeon mainshock, which correlates well with the negative static stress changes (i.e., stress shadow) cast by the mainshock. In comparison, the seismicity rate around Parkfield increased moderately where the static stress changes are positive. The seismicity rate changes correlate well with the static shear stress changes induced by the San Simeon mainshock, suggesting a low friction in the seismogenic zone along the Parkfield section of the San Andreas Fault.

Inspired by our above study around the 2003 San Simeon earthquake [Meng et al., 2013], we apply the same technique to a much wider region and much longer time window in central California. The goal is to systematically search for missing earthquakes in the entire central California from 01 June 2003 to 31 May 2005, which is ~6 months before the San Simeon earthquake to ~6 months after the 2004 Parkfield earthquake. With the more complete catalog, we are able to investigate how the two large events impacted the seismicity in central California and whether dynamic or static stress changes governed the triggering process. We are also interested in finding repeating earthquakes and examine potential variation in their occurrence intervals after a large event.

Background

The 2003 M_w6.5 San Simeon earthquake struck the central California coast on 22 December 2003, 19:15:56 UTC and induced large dynamic and static stress changes in its vicinity [*Hardebeck et al.*, 2004]. The mainshock ruptured a reverse fault striking northwest and dipping northeast and was followed by numerous aftershocks [*Hardebeck et al.*, 2004]. About nine months later, an M_w6.0 earthquake occurred on the Parkfield section of the San Andreas Fault (SAF), ~50 km to the east of the San Simeon mainshock epicenter (Figure 1a). Because the two earthquakes occurred closely in space and time, it is reasonable to speculate that the San Simeon mainshock may have triggered the Parkfield earthquake. Indeed, the Parkfield section of the SAF experienced positive Coulomb stress changes on the order of 10 kPa (Figure 1a), suggesting that the static stress changes may explain their triggering relationship [*Aron and Hardebeck*, 2009]. However, the seismicity rate around Parkfield decreased slightly after the San Simeon earthquake [*Aron and Hardebeck*, 2009], which is inconsistent with either the static Coulomb hypothesis and dynamic stress changes.

Previous studies on earthquake triggering mostly utilize existing earthquake catalogs, which may be incomplete immediately following large earthquakes, mainly due to the intensive seismic activity and masking from the coda waves of the mainshock and large aftershocks [*Aron and Hardebeck*, 2009; *Enescu et al.*, 2007; *Peng et al.*, 2007]. So, the seismicity rate decrease around

Parkfield could be due to the incompleteness of the Northern California Seismic Network (NCSN) catalog immediately after the San Simeon mainshock. Inspired by recent successes in detecting earthquakes and tectonic tremors based on the waveform matched filter technique [*Peng and Zhao*, 2009; *Shelly et al.*, 2007], we apply a modified version of this technique [*Meng et al.*, 2012] to systematically search for missing earthquakes around Parkfield using 13 borehole stations from High Resolution Seismic Network (HRSN), station PKD from Berkeley Digital Seismic Network (BK network) and 25 surface stations from Northern California Seismic Network (NC network) (Figure 1a and 1b). With a more complete catalog, we can elucidate the genuine seismicity rate changes along the SAF.

Research accomplished – Seismicity rate changes at Parkfield around the San Simeon mainshock [*Meng et al.*, 2013]

1. Data and Methods

The continuous seismic data are recorded by 39 stations from the HRSN, BK and NC network around Parkfield (Figure 1a and 1b). For HRSN stations, we use BP channels (short-period 3-component geophone recording at 20 sample/s). For station PKD, we use BH channels (broadband 3-component recording at 20 sample/s). For NC stations, we use the EHZ channel (short-period vertical component) down-sampled from 100 Hz to 20 Hz. Our study period is 90 days before to 90 days after the San Simeon earthquake. We use 3531 earthquakes listed in the relocated catalog [*Thurber et al.*, 2006] within 5 km to the SAF as template events (Figure 1a and 1b). These templates are the same with those used in a previous study [*Peng and Zhao*, 2009]. Templates waveforms are 1 s before and 5 s after the predicted *S*-wave arrival for two horizontal components, and 1s before and 5 s after the predicted *P*-wave arrival for the vertical component. The *P*- and *S*-wave arrival times are computed based on a 1D velocity model in this region [*Waldhauser et al.*, 2004].

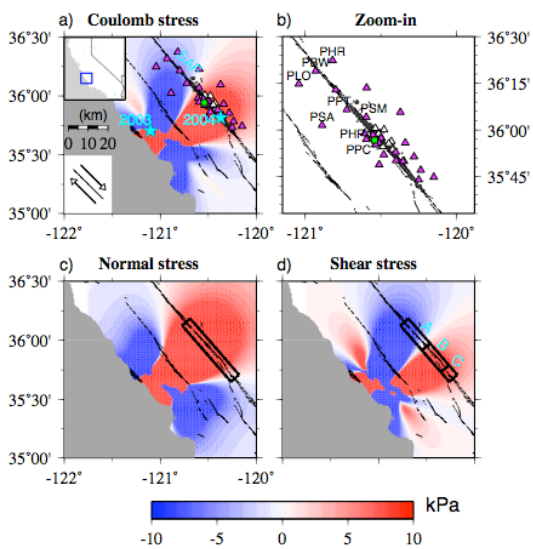

Figure 1. Map of central California. The color in the background represents static stress changes induced by the San Simeon earthquake at a depth of 7.5 km. (a) The grey dots represent 3531 template events. The white triangles represent 13 borehole stations in the HRSN. The magenta triangles represent 25 stations from NC network. The top left inset shows the map of California. (b) The zoom-in figure illustrates the relative location between stations and template events. (c) The black box marks our study region, the along-strike distance between 50 and 20 km relative to the epicenter of the 2004 Parkfield earthquake, and within 5 km to the SAF. (d) The boxes and letters denote three sub-regions.

We first apply a two-way 4th order band-pass filter of 2-8 Hz to both continuous and templates waveforms. Next, we compute the correlation-coefficient (CC) value in a 6-s time window between the template and continuous waveforms and move forward with a step of one data point (0.05 s). Then, we shift the CC values back to the origin time of the template event, stack and compute the mean CC value of all channels at each data point. A threshold is set for each mean CC trace, above which the positive correlation is considered as a detected event.

We compare the detecting time window of all positive detections, which is from the start time of the earliest correlating window to the end time of

the latest correlating window among all channels. If the detecting time windows of multiple detected events overlap, only the one with the highest CC value is kept and the corresponding template is referred to 'matching template' hereafter. The hypocenter of the 'matching template' is assigned to that of the detected event. The magnitude of the detected event is computed based on the median value of the peak amplitude ratio between the detected event and 'matching template' among all channels [*Peng and Zhao*, 2009]. Figure 2 illustrates an example of a positive detection at ~4 days after the San Simeon mainshock. The template event occurred on 2002/11/21 and had a magnitude of 1.09. The estimated magnitude for the newly detected event is 0.56.

2. False detections

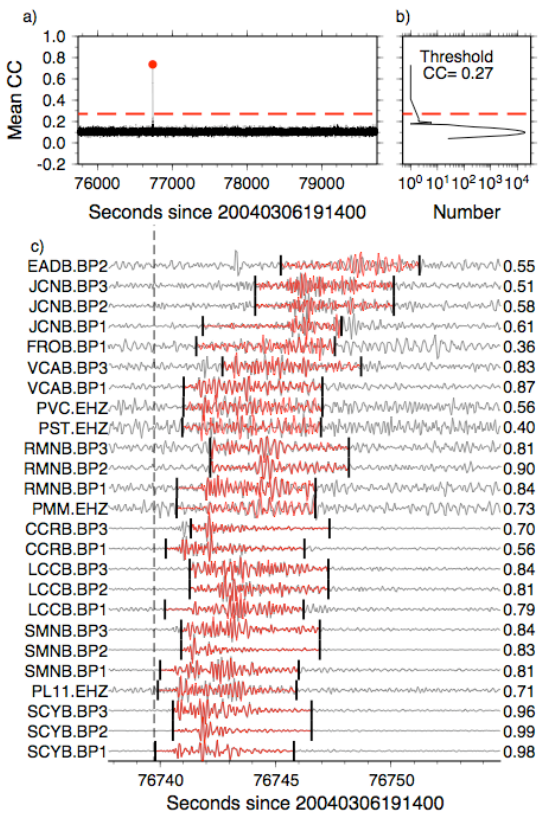

Figure 2. Example of a positive detection of an event near Parkfield after the San Simeon mainshock. (a) Mean CC trace versus seconds since 26 December 2003 at 19:14:00 for the template 20021121071116. The red dot corresponds to the detected event on 27 December 2003 02:25:25.10. (b) The histogram of the mean CC trace. (c) A comparison of the template waveforms (red) and the continuous waveforms (grey) around the origin time of the detected event which is marked as the red dot in (a). The vertical dashed line represents the origin time of the detected event. The solid black lines mark the time window used for waveform correlation for each channel.

Previous studies using the same technique generally define the threshold of positive detections as the sum of the median value and 8 or 9 times the median absolute deviation (MAD) of the mean CC trace [*Peng and Zhao*, 2009; *Shelly et al.*, 2007]. However, allowing one data point shift while stacking would lower the MAD value of mean CC trace. Hence a higher threshold should be applied in this study. We first select 12 times the MAD as threshold, which is roughly equivalent to 8 or 9 times the MAD in previous studies [*Peng and Zhao*, 2009; *Shelly et al.*, 2007].

Figure 3 illustrates a possible 'false detection' using the sum of median value and 12 times the MAD as threshold. The detected event occurred ~42 days after the San Simeon mainshock and was detected by a template beneath Middle Mountain with a mean CC value of 0.21. The correlated window of continuous waveforms appears to be a segment of seismic signals with much longer duration, indicating a distant source. According to the NCSN catalog, an aftershock of magnitude 1.46 occurred in the San Simeon rupture zone just ~7 s prior to this detection. We confirm that the event indeed is the San Simeon aftershock by predicting the *P*- and *S*-wave arrival times of the San Simeon aftershock at all stations. It appears that the template correlates with the *P*-wave train of the San Simeon aftershock. Hence, this kind of detection of a San Simeon aftershock is considered as 'false detections'.

As noted before, such 'false detections' have very low CC values. By increasing the threshold to be the sum of the median value and 15 times the MAD of mean CC trace, almost all the 'false detections' can be removed. 15 times the MAD in this study is roughly equivalent to 11 or 12 times the MAD in previous

studies. The selection of threshold is a tradeoff between the number of detected events and possibility of 'false detections'. By applying a higher threshold, we ensure that 'false detections' are discarded. However some local events might be excluded as well.

3. Results

Our primary study period for investigating seismicity rate changes is then chosen from 46 days before the mainshock, when the network change completed, to 31 days after the mainshock, when 8 NC stations stopped recording. Among 1664 detected events, 1046 events occurred during the primary study period. Figure 4a shows the locations of the 1046 detected events in cross-section along the SAF strike. Most of the detected events occurred beneath Stone Canyon (station SCYB) and Middle Mountain (station MMNB). In contrast, there were only a few

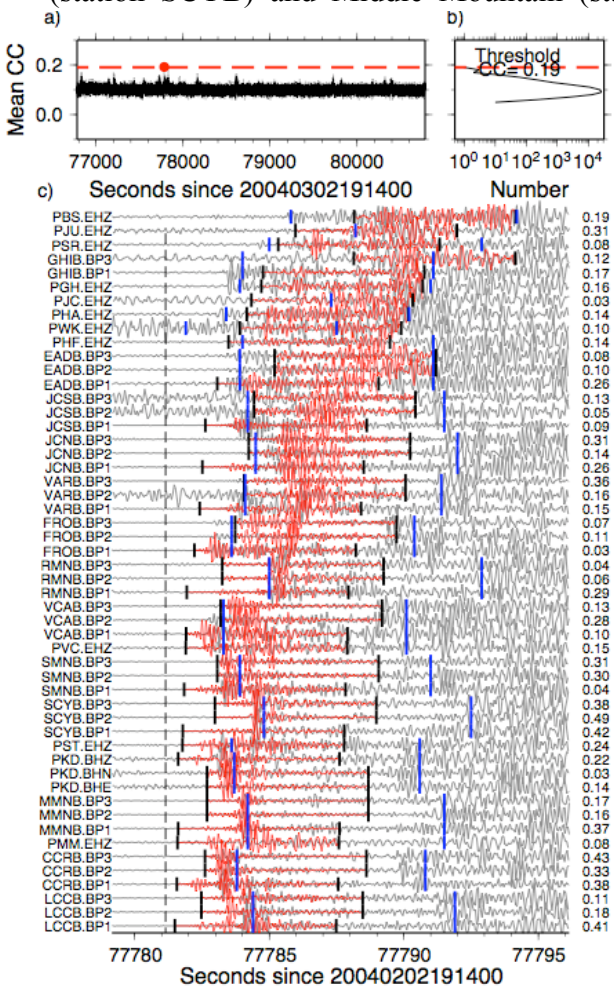

Figure 3. Example of a 'false detection' after the San Simeon mainshock. (a) Mean CC trace versus seconds since 2 February 2004 19:14:00 for the template 20040929004616. The red dot corresponds to the detected event. (b) The histogram of the mean CC trace. (c) The blue vertical lines denote the predicted *P*- and *S*-wave arrival times of one San Simeon aftershock occurred on 03 February 2004 16:50:14 listed in the NCSN catalog. Other denotations are the same as those in Figure 2.

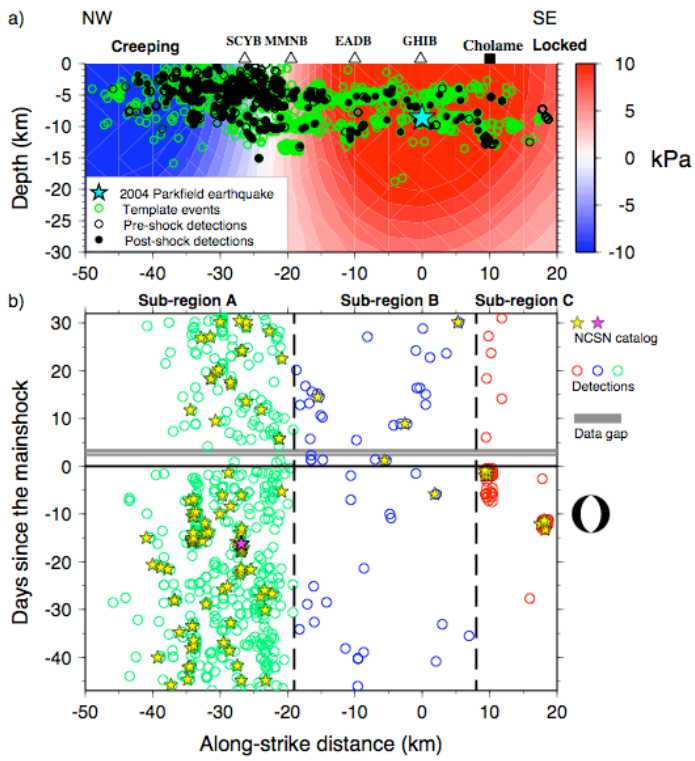

Figure 4. Spatio-temporal evolution of detected events from 46 days before to 31 days after the San Simeon earthquake. (a) The cross-section view of all templates (green) and detected events (black) along the SAF. The background contour denotes the static shear stress changes induced by the mainshock. (b) The origin times of all detected events relative to the mainshock (horizontal black line) versus their along-strike distances. The magenta star denotes the M_d2.77 earthquake occurred ~16 days before the mainshock. The beach ball denotes the focal mechanism of the first earthquake in the swarm occurred around the along-strike distance of 18 km.

detected events further northwest in the creeping section and southeast of Gold Hill (station GHIB) near Cholame.

3.1. Spatio-temporal Changes of Seismicity

The spatio-temporal evolution of the events shows a marked difference along the SAF strike (Figure 4b). Based on the distinct pre-shock behavior of seismicity, we divide our study area into three sub-regions and quantify the seismicity rate changes by computing β value, which is a measure of the difference between the observed number of events after the mainshock and the expected number from the background rate before the mainshock [*Aron and Hardebeck*, 2009]. We also compute the seismicity ratio, which is simply the ratio between the average post-mainshock rate and pre-mainshock rate [*Shelly and Johnson*, 2011]. We compute the magnitude of completeness (M_c) of -0.3, 0, and 0.6 for sub-region A, B, and C using the best-combined method in ZMAP [*Wiemer*, 2001], respectively. We recognize that the obtained M_c may be inaccurate and have temporal variations. Moreover, β value and seismicity ratio may strongly depend on M_c, hence we compute β value and seismicity ratio by setting the cutoff magnitude from -1.6 to 2 to avoid potential bias.

In sub-region A (northwest of Middle Mountain, less than −19 km in the along-strike distance), we find a clear seismicity rate decrease across all magnitude bands (Figure 5b and 5c). However, such a decrease may be caused by an abrupt jump in cumulative number ~16 days before the mainshock due to an M_d2.77 earthquake and its aftershocks (Figure 5a). To further evaluate this, we exclude the time window from the M_d2.77 earthquake to the San Simeon mainshock and re-calculate β value and seismicity ratio. For all magnitude bands, the decrease of seismicity rate is still significant at the 95% confidence level (i.e., $\beta < -2$) even after excluding the M_d2.77 earthquake sequence (Figure 5b). Moreover, we predict the expected decay of the aftershock sequence of the M_d2.77 earthquake after the San Simeon mainshock by fitting the modified Omori's law [*Utsu et al.*, 1995] using events that preceded the mainshock (Figure 5a). The aftershock sequence appeared to be slightly stifled by the San Simeon mainshock for ~30 days.

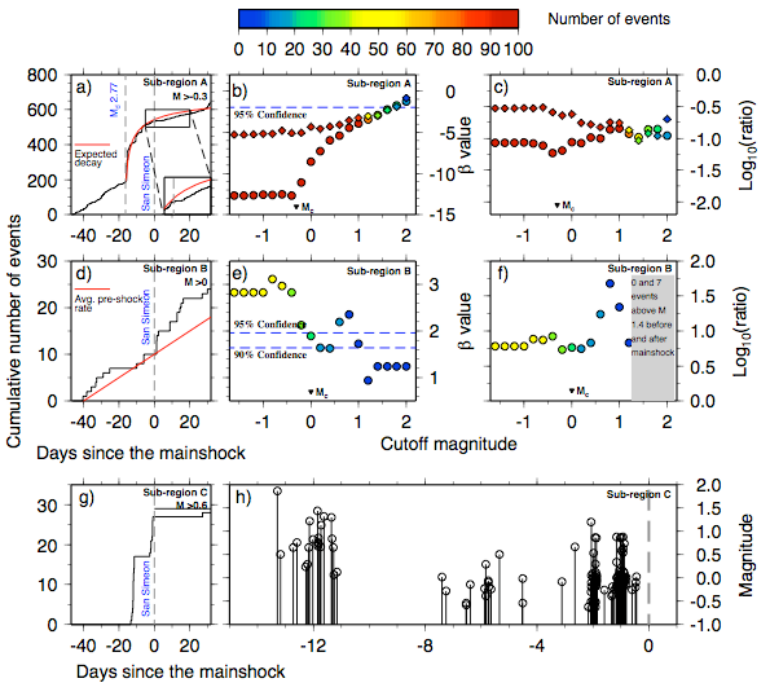

Figure 5. Cumulative numbers of earthquakes and corresponding statistical analysis in three sub-regions. (a), (d), and (g) The cumulative number of detected events above M_c in sub-region A, B and C versus days relative to the mainshock, respectively. (b) and (e) ḃvalues versus cutoff magnitude with detected events in sub-region A and B, respectively. Dots denote that background rate is measured prior to the San Simeon earthquake. Diamonds denote that background rate is measured prior to the M_d2.77 event. (c) and (f) The seismicity ratios versus cutoff magnitude with detected events in sub-region A and B, respectively. (h) The magnitude of detected earthquake swarms in sub-region C immediately before the mainshock.

The seismic activity changed dramatically across Middle Mountain. In sub-region B (between Middle

Mountain and Cholame, the along-strike distance between −19 km and 8 km), only 21 and 30 seismic events occurred before and after the mainshock, respectively (Figure 4b). A significant increase of seismicity rate is evident at the 90% confidence level for cutoff magnitude less than 0 (Figure 5e). For cutoff magnitude larger than 0, β values become statistically unreliable due to the small number of remaining events. The seismicity ratio increases for all cutoff magnitudes (Figure 5f).

In sub-region C (southeast of Cholame, with the along-strike distance of > 8 km), the seismicity was quiescent during most of our study period. A few swarms occurred at 15 and 10 days before the mainshock and completely stopped right before the origin time of the mainshock (Figure 4b). A dramatic decrease of seismicity rate is evident due to the earthquake swarms (Figure 5g and 5h). However, if we remove the swarm sequences, 2 and 6 events remained before and after the mainshock, respectively. We do not compute β value or seismicity ratio with only 8 events. Nevertheless, a moderate increase of seismicity rate after the mainshock can be inferred without the swarms.

4. Comparisons with the Static Stress Changes

We calculate the static stress changes produced by the San Simeon earthquake based on an updated finite fault model [*Ji et al.*, 2004]. Here we calculate the shear, normal and Coulomb stress changes at 7.5 km depth in map view (Figure 1) and along the strike in cross-section (Figure 4a) with an effective coefficient of friction of 0.4 [*Aron and Hardebeck*, 2009]. The 7.5 km depth is chosen to be close to the average depth of the detected events.

No apparent consistency between the Coulomb stress and seismicity rate changes is found. Instead, static shear stress changes alone explain the behavior of seismicity across our study region. In particular, a clear negative static shear stress (i.e., stress shadow) is found in the creeping section of the SAF (sub-region A). We also observe a significant decrease of seismicity rate across all magnitude bands (Figure 5) and a stifled aftershock sequence of an M_d2.77 earthquake (Figure 5a), consistent with the stress shadow effect. An abrupt recovery at ~30 days after the mainshock can be seen for our detected events (Figure 5a). In comparison, between Middle Mountain and Cholame the static shear stress increased after the San Simeon mainshock, and we find a moderate increase of seismic activity for most magnitude bands (Figure 5d-f).

5. Discussion

In this study, we applied the waveform matched filter technique to detect earthquakes around the Parkfield section of the SAF following the nearby San Simeon mainshock. After removing all possible false and duplicated detections, we have detected ~8 times more events than listed in the NCSN catalog. The seismicity rate beneath the creeping section of the SAF showed a statistically significant reduction following the San Simeon mainshock, which correlates well with the negative shear stress changes. Interestingly, deep tectonic tremors in that sub-region were also stifled for 3-6 weeks and followed by an accelerated recovery from ~30 days after the mainshock, which agrees well with estimated duration of the stress shadow effect [*Shelly and Johnson*, 2011]. However, the recovery of earthquake activity in this study was transient and the seismicity rate remained low near the end of our study period. The seismicity rate increased moderately in sub-region B around the rupture zone of the 2004 Parkfield earthquake (Figure 5e and 5f), where positive static shear stress changes were induced (Figure 4a), suggesting that the San Simeon mainshock loaded this section of the SAF. This is also consistent with the triggered creep events near Parkfield on the SAF observed by the USGS

creep meters after the San Simeon mainshock [*Aron and Hardebeck*, 2009] and a minor increase of tremor activity in the lower crust [*Shelly and Johnson*, 2011].

The seismicity rate changes at Parkfield correlates well with the static shear stress changes induced by the San Simeon earthquake, suggesting that static stress change is an important, if not the only, agent for near-field triggering in this region. Our results are consistent with a recent finding of a stress shadow in the aftershock zone of the 1992 M_w6.3 Joshua Tree earthquake cast by the 1992 M_w7.3 Landers earthquake [*Toda et al.*, 2012], indicating that stress shadows do exist and may play an important role in changing seismic activities in the near field. Transient dynamic triggering may have occurred in our study region, but was not detected by our technique because of the close distance between Parkfield and the San Simeon epicenter, and clipping of the stations in the first ~100 s immediately after the San Simeon mainshock.

The fact that static shear stress, instead of Coulomb stress, changes were consistent with the seismicity rate changes, as well as the behavior of tectonic tremors [*Shelly and Johnson*, 2011], argues for a very low friction along the Parkfield section of the SAF through the entire crust. This was also suggested by the laboratory measurement from SAFOD drilling samples [*Lockner et al.*, 2011] and previous study on response of the Parkfield section of the SAF to large earthquake [*Toda and Stein*, 2002]. Such fault weakness may attribute to the fact that the mature SAF developed a thick, impermeable gauge zone that reduces the effective coefficient of friction.

Research accomplished – Systematic detections of triggered earthquakes in Central California [Meng et al., 2012b]

Inspired by our recently published work [*Meng et al.*, 2013], we apply the same technique to a much wider region and much longer time window. Here we use ~50,000 earthquakes listed in the Northern California Seismic Network (NCSN) catalog from 1984 to 2009 as template events (Figure 6). The waveforms are recorded by 147 NC stations. The continuous seismic recordings are ~660 days long and ~1 TB in size. Both template and continuous waveforms are band-pass filtered from 2 to 8 Hz. The detection procedure generally follows that of [*Peng and Zhao*, 2009; *Meng et al.*, 2013]. Because of the enormous amount of data, we use a recently developed GPU version of the matched filter code [*Meng et al.*, 2012a] and processed data on a supercomputing cluster, 'Keeneland' (http://keeneland.gatech.edu/). This approach helps decrease the running time from months to a few days. Figure 7 shows an example of a possible repeating event detected ~40 minutes after the Parkfield earthquake by a template event in 1991. The correlation coefficient (CC) is 0.93.

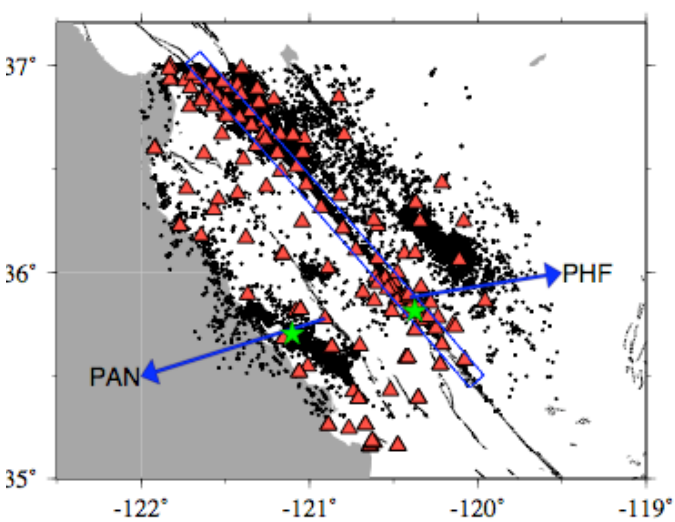

Figure 6. Map of central California. The black dots mark the hypocenters of ~70,000 template events. The red triangles mark the 147 NC stations. The green stars mark the hypocenters of the 2003 San Simeon and 2004 Parkfield earthquake. The blue box marks the region where seismicity rate changes are calculated in Figure 8.

Using 12 times the median absolute deviation (MAD) as threshold, we detect ~70,000 earthquakes, which are roughly 4 times more than the NCSN catalog. Figure 8 show the significant increase of triggered

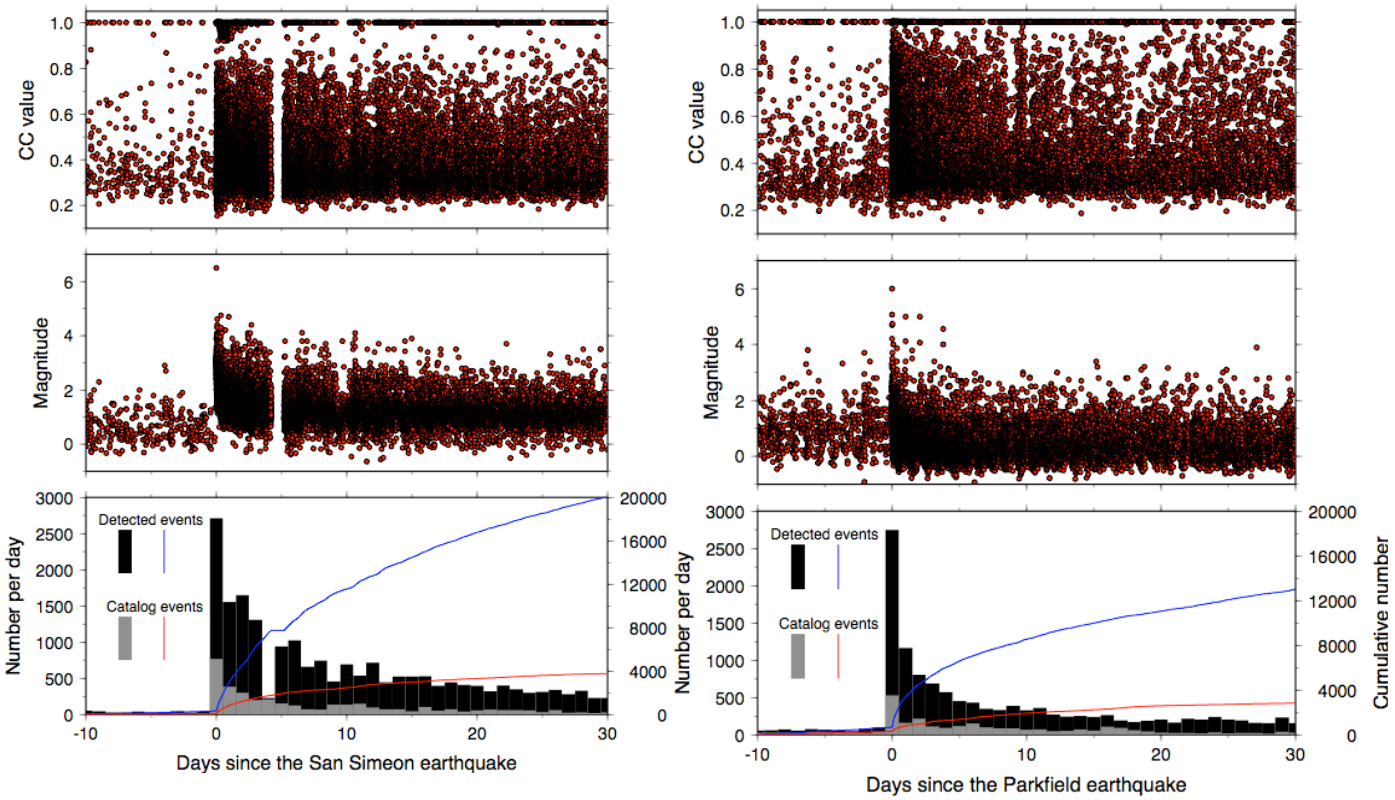

Figure 7. (Left) Cross-correlation values (top) and magnitudes (middle) of detected events versus days relative to the San Simeon mainshock, respectively. (Bottom) Comparison of seismicity rate between our detected events and NCSN catalog. (Right) Same with left except with events detected around the origin time of the Parkfield mainshock.

earthquakes comparing with the NCSN catalog in 30 days following the San Simeon and Parkfield mainshock, respectively.

Previously, [*Meng et al.*, 2013] found that the seismicity rate changes pattern near Parkfield section along the SAF were consistent with the static shear stress changes induced by the San Simeon mainshock, which suggests that static triggering was the dominant triggering mechanism. Here, with the updated catalog for entire central California, we are able to examine the seismicity rate changes in a much larger section along the SAF (Figure 6). In creeping section of the SAF, where static shear stress decreased, the seismicity rate became significant lower than the pre-shock level immediately following the San Simeon mainshock (Figure 8). In particular, the seismicity in creeping section seems devoid in the first a few days after the mainshock. This observation further confirms the existence of 'stress shadow' in creeping section along the SAF, which is observed by [Meng et al., 2013] and [Shelly and Johnson, 2011]. Across the static shear stress changes boundary, the seismicity rate changes are identical with that of [Meng et al., 2013]. Near the epicenter of the Parkfield earthquake, the seismicity rate moderately increased after the San Simeon mainshock. Further southeast, a few swarms stopped right before the San Simeon mainshock and hence caused a significant decrease of seismicity. In locked section of the SAF, no event is detected 50 days before to 100 days after the mainshock.

Conclusions

We have successfully applied the waveform matching technique to detect missing earthquakes in central California following the 2003 Mw6.5 San Simeon and 2004 Mw6.0 Parkfield earthquake [Meng et al., 2013, 2014]. These newly detected events have helped us to

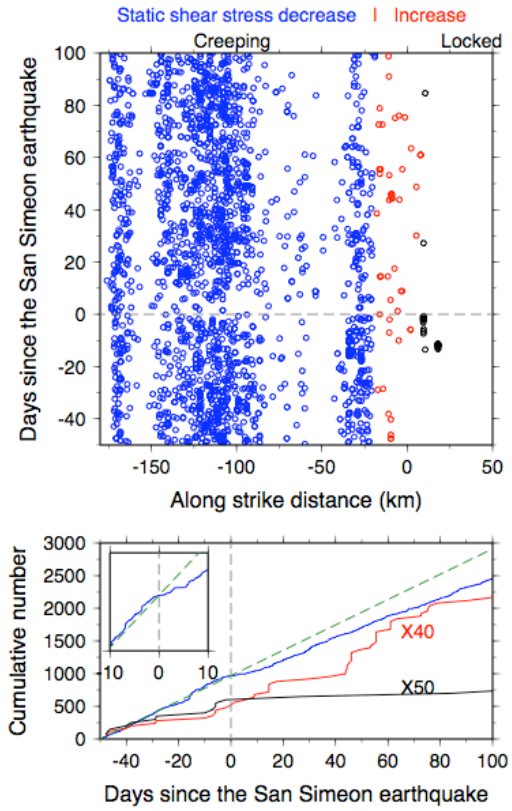

Figure 8. (Top) Temporal-spatial relationship of detected events along the SAF. (Bottom) Cumulative number of detected events in three sub-regions. The green dashed line marks the pre-shock level in creeping section. Inset figure illustrates the seismicity rate changes in creeping section immediately before and after the San Simeon mainshock.

better understand the triggering mechanism in this region. In particular, we found a statistically significant decrease of seismicity along the creeping section of the San Andreas Fault following the San Simeon mainshock, which correlates well with the negative static stress changes (i.e., stress shadow) cast by the mainshock. In comparison, the seismicity rate around Parkfield increased moderately where the static stress changes are positive. The seismicity rate changes correlate well with the static shear stress changes induced by the San Simeon mainshock, suggesting a low friction in the seismogenic zone along the Parkfield section of the San Andreas Fault. Our next step is to finish examining the effects of the 2004 Parkfield earthquake on the aftershock decay patterns in the rupture zone of the 2003 Mw6.5 San Simeon earthquake.

Bibliography of published work

1. Meng*, X., Z. Peng, and J. Hardebeck (2013), Seismicity around Parkfield correlates with static shear stress changes following the 2003 Mw6.5 San Simeon earthquake, *J. Geophys. Res.*, 118(7), 3576-3591, doi:10.1002/jgrb.50271.
2. Meng, X., Z. Peng, J. L. Hardebeck, X. Yu, and B. Hong (2012b), Systematic search for missing earthquakes in Central California around the 2003 Mw6.5 San Simeon and the 2004 Mw6.0 Parkfield earthquakes, Abstract S54A-01 presented at 2012 Fall Meeting, AGU, San Francisco, Calif., 3-7 Dec.
3. Meng*, X., X. Yu, Z. Peng and B. Hong (2012a), Detecting earthquakes around Salton Sea following the 2010 M_w7.2 El Mayor-Cucapah earthquake using GPU parallel computing, *Procedia Computer Science*, 9, 937-946.

References

Aron, A., and J. Hardebeck (2009), Seismicity rate changes along the central california coast due to stress changes from the 2003 m 6.5 san simeon and 2004 m 6.0 parkfield earthquakes, *B Seismol Soc Am*, *99*(4), 2280-2292.

Enescu, B., J. Mori, and M. Miyazawa (2007), Quantifying early aftershock activity of the 2004 mid-niigata prefecture earthquake (m(w)6.6), *Journal of Geophysical Research-Solid Earth*, *112*(B4).

Hardebeck, J., et al. (2004), Preliminary report on the 22 december 2003, m 6.5 san simeon, california earthquake, *Seismol Res Lett*, *75*(2), 155-172.

Harris, R., and R. Simpson (1992), Changes in static stress on southern california faults after the 1992 lander earthquake, *Nature*, *360*(6401), 251-254.

Ji, C., K. Larson, Y. Tan, K. Hudnut, and K. Choi (2004), Slip history of the 2003 san simeon earthquake constrained by combining 1-hz gps, strong motion, and teleseismic data, *Geophys Res Lett*, *31*(17).

Lockner, D., C. Morrow, D. Moore, and S. Hickman (2011), Low strength of deep san andreas fault gouge from safod core, *Nature*, *472*(7341), 82-U107.

Peng, Z., and P. Zhao (2009), Migration of early aftershocks following the 2004 parkfield earthquake, *Nat Geosci*, *2*(12), 877-881.

Peng, Z., J. Vidale, M. Ishii, and A. Helmstetter (2007), Seismicity rate immediately before and after main shock rupture from high-frequency waveforms in japan, *Journal of Geophysical Research-Solid Earth*, *112*(B3).

Shelly, D., and K. Johnson (2011), Tremor reveals stress shadowing, deep postseismic creep, and depth-dependent slip recurrence on the lower-crustal san andreas fault near parkfield, *Geophys Res Lett*, *38*.

Shelly, D., G. Beroza, and S. Ide (2007), Non-volcanic tremor and low-frequency earthquake swarms, *Nature*, *446*(7133), 305-307.

Thurber, C., H. Zhang, F. Waldhauser, J. Hardebeck, A. Michael, and D. Eberhart-Phillips (2006), Three-dimensional compressional wavespeed model, earthquake relocations, and focal mechanisms for the parkfield, california, region, *B Seismol Soc Am*, *96*(4), S38-S49.

Toda, S., and R. Stein (2002), Response of the san andreas fault to the 1983 coalinga-nunez earthquakes: An application of interaction-based probabilities for parkfield, *Journal of Geophysical Research-Solid Earth*, *107*(B6).

Toda, S., R. Stein, G. Beroza, and D. Marsan (2012), Aftershocks halted by static stress shadows, *Nat Geosci*, *5*(6), 410-413.

Utsu, T., Y. Ogata, and R. S. Matsuura (1995), The centenary of the omori formula for a decay law of aftershock activity, *Journal of Physics of the Earth*, *43*(1), 1-33.

Waldhauser, F., W. Ellsworth, D. Schaff, and A. Cole (2004), Streaks, multiplets, and holes: High-resolution spatio-temporal behavior of parkfield seismicity, *Geophys Res Lett*, *31*(18).

Wiemer, S. (2001), A software package to analyze seismicity: Zmap, *Seismol Res Lett*, *72*, 373-382.